ACS Catalysis

Research Article

pubs.acs.org/acscatalysis

Redispersion of Gold Supported on Oxides

Jacinto Sá,[†,‡] Sarah Frances Rebecca Taylor,[†] Helen Daly,[†] Alexandre Goguet,[†] Ramchandra Tiruvalam,[§] Qian He,[§] Christopher J. Kiely,[§] Graham J. Hutchings,[⊥] and Christopher Hardacre[†,*]

[†]School of Chemistry and Chemical Engineering, David Keir Building, Queen's University Belfast, Stranmillis Road, Belfast, BT9 5AG, Northern Ireland, U.K.

[‡]Paul Scherrer Institute, 5232 Villigen PSI, Switzerland

[§]Department of Materials Science and Engineering, Lehigh University, 5 East Packer Avenue, Bethlehem, Pennsylvania 18015-3195, United States

[⊥]Cardiff Catalysis Institute, School of Chemistry, Cardiff University, CF10 3AT, Cardiff, U.K.

Supporting Information

ABSTRACT: Although many gold heterogeneous catalysts have been shown to exhibit significant activity and high selectivity for a wide range of reactions in both the liquid and gas phases, they are prone to irreversible deactivation. This is often associated with sintering or loss of the interaction of the gold with the support. Herein, we report on the use of methyl iodide as a method of dispersing gold nanoparticles supported on silica, titania, and alumina supports. In the case of titania- and alumina-based catalysts, the gold was transformed from nanometer particles into small clusters and some atomically dispersed gold. In contrast, although there was a drop in the gold particle size on the silica support following CH_3I treatment, the size remained in the submicrometer range. The structural changes were correlated with changes in the selectivity and activity for ethanol dehydration and benzyl alcohol oxidation. From these observations, it is clear that this treatment provides a method by which deactivated gold catalysts can be reactivated via redispersion of the gold.

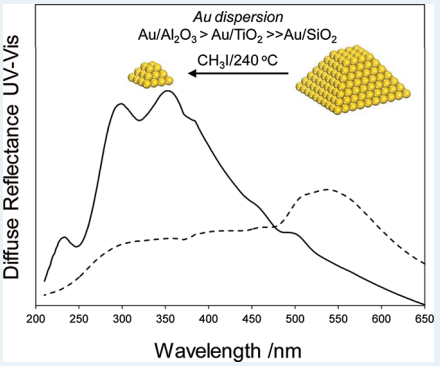

KEYWORDS: *gold, redispersion, methyl iodide, oxides, dehydration, oxidation*

INTRODUCTION

Gold-based catalysts have been examined extensively over the last three decades due to their high selectivity and activity for a wide range of reactions.[1] Haruta et al.[2] and Hutchings et al.[3] initially developed gold-based systems for low-temperature CO oxidation and acetylene hydrochlorination, demonstrating that heterogeneous catalysts based on gold were active. Thereafter, gold has been shown to be effective for hydrogenations,[4] selective oxidations,[5] hydroaminations[6] and epoxidations,[7] and environmental remediation[8] and in bulk/fine chemicals applications.[9]

The transformation of gold from an inert metal to one that is catalytically active is due to the production of small nanoparticles and the nature of their interaction with the support used with both the size of the particles and the specific support used important in the activities and selectivities observed.[10−12] Although many gold catalysts are highly active initially, many undergo irreversible deactivation, even under benign conditions, and therefore, methods by which they can be stabilized or reactivated are particularly important in this field. Typical causes of deactivation include particle sintering or loss of metal−support interaction.[13] In contrast, Eastman Chemicals demonstrated that gold supported on carbon could be activated online during the high pressure carbonylation of methanol to methyl acetate.[14] This activation of the gold has been demonstrated to be due to an increase in the dispersion of the gold nanoparticles from >10 nm clusters to atoms and dimers of gold stabilized by iodine.[15] In this case, the presence of methyl iodide in the reaction mixture leads to the structural transformation, albeit at 240 °C and 16 bar.

Sá et al.[16] recently investigated the dispersion process of gold nanoparticles supported on activated carbon and graphite using CH_3I treatments at atmospheric pressure and temperatures between 50 and 240 °C. Therein, an atomic dispersion of gold was achieved at temperatures as low as 50 °C. The proposed reaction mechanism suggested that gold is initially oxidized by interaction with iodine, followed by dissociation of Au−I entities from the central particle. The much more benign conditions used to disperse the catalyst, in this case, provides an opportunity to redisperse gold supported on carbon following sintering as a routine procedure to reactivate catalysts.

Although many reactions make use of gold supported on carbon based supports, a large number of reactions are catalyzed by gold supported on metal oxides, with alumina,

Received: January 30, 2012
Revised: March 1, 2012
Published: March 2, 2012

 © 2012 American Chemical Society

silica, and titania being the most commonly used. In the present study, the general applicability of the CH_3I treatment for the dispersion of gold particles supported on oxides has been examined. In this case, the interaction of the metal nanoparticles with the metal oxide supports is stronger than in the case of carbon based supports, and therefore, redispersion of the Au presents a more significant challenge.

EXPERIMENTAL SECTION

Catalyst Preparation and CH_3I Treatment. Hydrogen tetrachloroaurate trihydrate ($HAuCl_4{\cdot}3H_2O$; Alfa Aesar), γ-Al_2O_3 (Johnson Matthey), TiO_2 (Degussa, P25), and SiO_2 (Aldrich) were used as received. Silica-, alumina-, and titania-supported Au catalysts were prepared by wet impregnation. Typically, a suspension of the support was prepared in distilled water, and under stirring, a solution of $HAuCl_4{\cdot}3H_2O$ of the required concentration was added dropwise into the support suspension. Subsequently, the resultant solid was dried overnight (~100 °C) and reduced under a flow of 5% H_2/Ar (30 cm^3 min^{-1}) for 2 h at 300 °C. For all the catalysts prepared, the gold loading was nominally set at 1.5 wt %. The actual metal loadings as measured by ICP−MS (ion coupled plasma−mass spectroscopy) for all fresh and CH_3I-treated catalysts are summarized in Table 1. Two additional reference catalysts supplied by the World Gold Council (WGC) were also examined: namely, 0.8 wt % Au/TiO_2 and 0.9 wt % Au/Al_2O_3.[17]

Table 1. Sample Notation and Summary of Bulk and Surface Concentration of Gold Measured by ICP and XPS, Respectively, As Well As Surface Concentration of Iodine Measured by XPS, and the Binding Energy (BE) of the Au $4f_{7/2}$ Peak for the Fresh and CH_3I-Treated Catalysts

sample	material	treatment	ICP Au (wt %)	XPS Au (at. %)	XPS I (at. %)	BE Au $4f_{7/2}$ (eV)
0.8Ti-fresh	0.8 wt % Au/TiO_2	fresh	0.8	2.1	0.0	82.9
0.8Ti-CH_3I		CH_3I	0.6	1.7	7.3	84.4
1.7Ti-fresh	1.7 wt % Au/TiO_2	fresh	1.7	1.8	0.0	82.9
1.7Ti-CH_3I		CH_3I	1.7	1.6	9.1	83.6
0.9Al-fresh	0.9 wt % Au/Al_2O_3	fresh	0.9	0.9	0.0	*a*
0.9Al-CH_3I		CH_3I	0.9	0.3	15.6	*a*
2.0Al-fresh	2.0 wt % Au/Al_2O_3	fresh	2.0	0.5	0.0	83.1
2.0Al-CH_3I		CH_3I	1.6	2.8	13.5	84.3
1.3Si-fresh	1.3 wt % Au/SiO_2	fresh	1.3	0.4	0.0	83.8
1.3Si-CH_3I		CH_3I	1.3	0.4	0.0	83.8

[a]XPS peaks were too small and ill-defined to obtain quantitatively meaningful values.

All CH_3I (Aldrich) treatments were performed in a glass reactor (o.d. 10 mm) using ~250 mg of catalyst and a steady flow of 40 cm^3 min^{-1} CH_3I/Ar with the vapor pressure of the CH_3I determined by a saturator held at 25 °C, equating to 0.14 cm^3 min^{-1} of CH_3I. The glass reactor was heated in flowing Ar within a tubular furnace, and the temperature was increased to the set temperature (240 °C) using a ramp rate of 10 °C min^{-1}, followed by a dwell time at this set temperature of 1 h. Once at the desired temperature, the CH_3I/Ar mixture was admitted to the reactor.

Characterization. XPS analysis was performed with a Kratos AXIS Ultra DLD apparatus, equipped with monochromated Al K_α radiation X-ray source, a charge neutralizer, and a hemispherical electron energy analyzer. During data acquisition, the chamber pressure was kept below 10^{-9} mbar. All spectra were averaged over 100 sweeps for Au 4f and 30 sweeps for all other elements of interest, with a step size of 0.1 eV, dwell time of 200 ms, and pass energy of 160 eV. The spectra were analyzed using the CasaXPS software pack and corrected for charging using C 1s binding energy (BE) as the reference at 284.6 eV.

Diffuse reflectance ultraviolet−visible spectroscopy measurements were performed in a Lambda 650S UV−vis spectrophotometer equipped with a Harrick high-temperature reaction chamber and an integrating sphere detector. MgO was used as a background spectrum, and the experiments were performed under a flow of Ar (30 cm^3 min^{-1}) at room temperature. Powder X-ray diffraction measurements were carried out using a PANalytical X'Pert Pro X-ray diffractometer. The X-ray source used was Cu K_α with a wavelength of 1.5405 Å. Diffractograms were typically collected from 30° to 60° with a step size of 0.03°. Inductively coupled plasma (ICP) using a Perkin−Elmer Optima 4300 was used to quantify the amount of Au present before and after each CH_3I treatment. Sodium peroxide fusion was used to strip the gold from the support.

Atomic-resolution, high-angle annular dark field (HAADF) scanning transmission electron microscopy (STEM) characterization was carried out using a 200 kV JEOL 2200FS TEM/STEM equipped with CEOS spherical aberration corrector. All STEM-HAADF images were light low-pass-filtered using a 3 × 3 kernel to reduce high-frequency noise. For TEM/STEM analysis, the sample was prepared by dry dispersing the catalyst powder material on a holey-carbon film supported by a 300-mesh copper TEM grid. Particle size histograms were constructed from the analysis of several hundred particles. Specimens for scanning electron microscopy (SEM) analysis were prepared by dry dispersing the powder onto conductive carbon tape attached to an Al stub. The SEM instrument used in this study was a Hitachi 4300SE/N equipped with a Schottky field emission gun. The backscattered electron (BSE) imaging mode was used in the SEM to highlight the heavier-metal-containing component against the support material.

Reactions. Benzyl alcohol oxidation was carried out at 80 °C and atmospheric pressure in a 250 cm^3, three-necked, round-bottom flask fitted with a reflux condenser, oil bath, thermocouple, and magnetic stirrer. Typically, 80 cm^3 of toluene, 80 μL of benzyl alcohol, and 40 μL of decane (internal standard) were added to the round-bottom flask, and oxygen was bubbled through the liquid. Once the temperature was stable at 80 °C, 0.075 g of catalyst was added to the reaction mixture. Samples of the liquid mixture were collected at regular intervals over a period of 4 h of reaction time and analyzed by GC (Agilent 6890N equipped with a flame ionization detector, and a ZB-5 (Zebron) column with helium as the carrier gas).

Gas phase ethanol dehydrogenation was performed in a quartz tubular reactor (o.d. 6 mm). Typically, 20 mg of catalyst was used, which was held in place between two plugs of quartz wool, and a thermocouple was placed in the center of the

dx.doi.org/10.1021/cs300074g | ACS Catal. 2012, 2, 552−560

catalyst bed. An Ar flow was passed through a saturator with pure ethanol set at ~5 °C to provide 1 vol % of concentration of reactant in the feed (total flow rate of 15 cm^3 min^{-1}). The temperature of the reactor was controlled using a tubular furnace with a PID controller and set at 400 °C. Prior to the catalytic tests, the catalysts were treated in a feed of Ar (15 cm^3 min^{-1}) for 30 min at 400 °C. The reactants and products were analyzed by mass spectrometry (Pfeiffer Vacuum OmniStar) at the outlet of the reactor.

RESULTS AND DISCUSSION

The ICP and XPS characterization results for the fresh and CH_3I-treated titania-, alumina-, and silica-supported gold catalysts are summarized in Table 1. The ICP measurements showed that the CH_3I treatment did not significantly affect the gold loading, with only small changes in gold content being observed for the 0.8 wt % Au/TiO_2 and 2.0 wt % Au/Al_2O_3 catalysts. This is consistent with the previously reported data on carbon-based catalysts in which little leaching/removal of gold was observed, even at 240 °C. In contrast, the XPS measurements showed a slight decrease in the Au atomic abundance after the CH_3I treatment for all catalysts, with the exception of the 2.0 wt % Au/Al_2O_3 catalyst. For all materials, this effect is correlated with the appearance of iodine on the spectra due to the treatment. Surprisingly, no iodine was detected for the silica catalyst after treatment. In the case of the titania- and alumina-supported catalysts, the CH_3I treatment led to an increase of ~1 eV in the gold binding energy, suggesting gold oxidation from the metallic to the +1 state, probably resulting from the formation of Au−I ensembles.[18] This result is consistent with the observation made for the gold catalysts supported on activated carbon and graphite.[16,16]

Diffuse reflectance UV−vis (DR-UV−vis) spectra of the titania-, alumina-, and silica-based catalysts before and after CH_3I treatment are reported in Figures 1, 2, and 3, respectively. The 0.8 wt % Au/TiO_2 sample showed two broad peaks at ~550 and 410 nm as well as a shoulder at 350 nm before treatment. Upon CH_3I treatment, the peak at 550 nm decreased and the other two features increased. The same trend was also observed for the 1.7 wt % Au/TiO_2 catalyst. From previously reported DR-UV−vis of supported gold particles,[19−21] the band at 200−250 nm is assigned to isolated Au ions, whereas the bands between 280 and 380 nm have been attributed to the partially charged Au_n ($1 < n < 10$) clusters.[19,20] The bands above 550 nm were ascribed to larger Au^0 particles.[19,21] Therefore, the DR-UV−vis spectra of the TiO_2-based catalysts suggest that in both cases, the fresh sample is dominated by large ensembles, nanoparticles with some small gold clusters also present, or both. Following CH_3I treatment, the bands due to the small clusters increase at the expense of larger nanoparticles. Unfortunately, because of the absorptive behavior of the TiO_2 support below 330 nm, it was not possible to detect the presence of isolated atoms, a species which was commonly observed in the case of CH_3I-treated gold supported on carbon.[14,14]

In the case of the 0.9 wt % Au/Al_2O_3 catalyst, the DR-UV−vis spectrum was dominated by two broad peaks at 550 and 290 nm. Upon CH_3I treatment, the spectrum changed, and three sharp peaks located at 225, 280, and 380 nm were observed. The same trend was observed for the 1.5 wt % Au/Al_2O_3 catalyst, with the only noticeable difference being that the spectrum of the fresh catalyst showed a more pronounced peak at 550 nm compared with that associated with the 0.9 wt % Au/Al_2O_3 catalyst, indicating a larger proportion of Au particles for the higher loaded sample. The spectral changes observed imply that the CH_3I treatment led to an almost complete redispersion of the large nanoparticles initially present in the fresh alumina-based samples into small clusters and isolated ions.

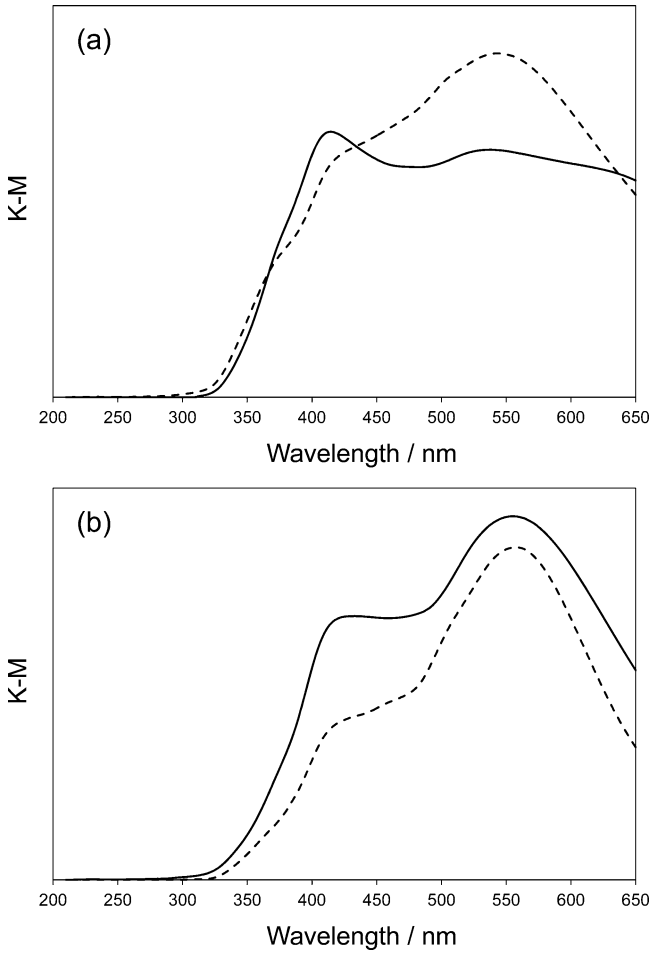

Figure 1. Diffuse reflectance UV−vis spectra of the (a) 0.8 wt % Au/TiO_2 and (b) 1.7 wt % Au/TiO_2 catalysts before (dashed line) and after (solid line) CH_3I treatment.

The silica-based catalysts show features before and after CH_3I treatment that are similar to that observed for the alumina supported catalysts, with peaks located at around 275, 390, and 510 nm, the major difference observed between the alumina and silica supports being the appearance of a sharp peak at around 220 nm after the CH_3I treatment. This result suggests some dissolution of the large particles and clusters into isolated ions upon CH_3I treatment.

To get a more in-depth characterization of the treated samples, XRD analysis was performed for the higher loading catalysts and HAADF-STEM imaging for the subset of WGC catalysts (0.8 wt % Au/TiO_2 and 0.9 wt % Au/Al_2O_3) and the 1.3 wt % Au/SiO_2 materials. Figure 4 shows mass- (Z-) contrast HAADF images of the 0.8 wt % Au/TiO_2 catalyst in the fresh and CH_3I-treated states. The "as-received" 0.8 wt % Au/TiO_2 catalyst (Figure 4a and b, and Supporting Information Figure S1) consisted primarily of 1−6 nm (mean size 2.8 nm) nanoparticles dispersed homogeneously over the support. In contrast, when this material was treated with CH_3I, the mean size of the particles was practically unchanged, but the sample showed an order of magnitude drop in the number density per

dx.doi.org/10.1021/cs300074g | ACS Catal. 2012, 2, 552−560

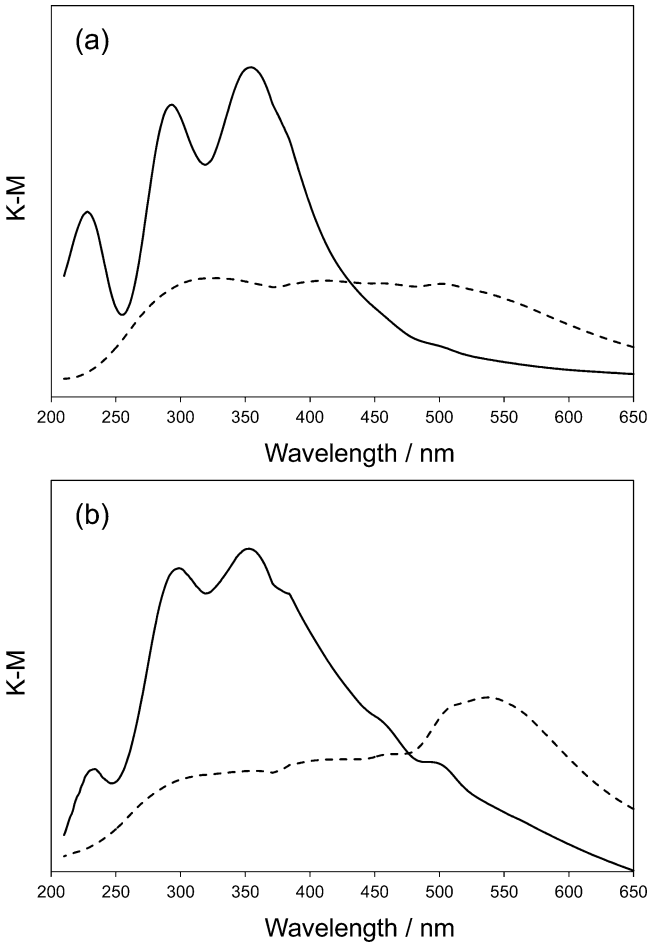

Figure 2. Diffuse reflectance UV−vis spectra of the (a) 0.9 wt % Au/Al_2O_3 and (b) 2.0 wt % Au/Al_2O_3 catalysts before (dashed line) and after (solid line) CH_3I treatment.

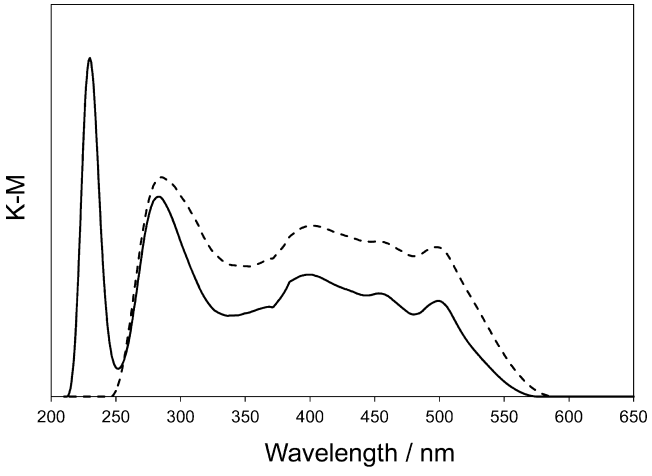

Figure 3. Diffuse reflectance UV−vis spectra of the 1.3 wt % Au/SiO_2 catalyst before (dashed line) and after (solid line) CH_3I treatment.

unit area of these nanoparticles, as shown in Figure 4c and Supporting Information Figure S2. This was due to the redispersion of some particles over the support as much smaller species as well as some, albeit small, loss of Au during the CH_3I treatment, as noted from the ICP results on this particular sample (Table 1). Furthermore, the CH_3I-treated sample also showed direct evidence for the presence of some Au clusters

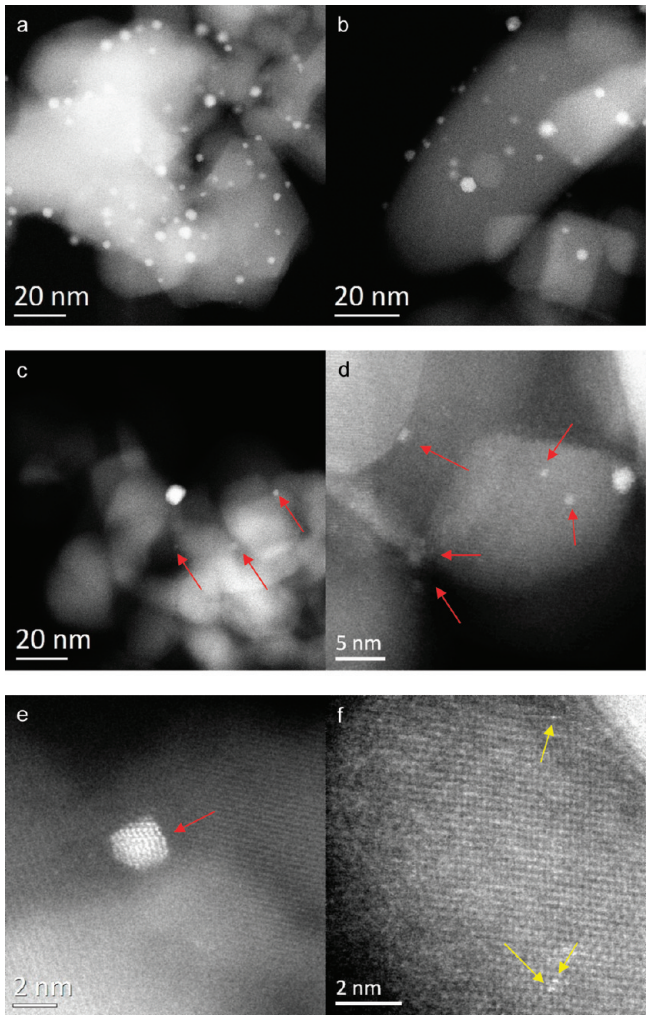

Figure 4. (a, b) Representative HAADF STEM images of the fresh 0.8 wt % Au/TiO_2 catalyst showing just 2−6 nm nanoparticles. (c−f) Corresponding images of the CH_3I-treated 0.8 wt % Au/TiO_2 material. A drastically decreased Au nanoparticle density compared with the untreated catalyst is noted. Small 0.5−2.0 nm Au clusters are indicated with red arrows. Some individual Au atoms can just about be detected on the crystalline TiO_2 support (yellow arrows).

and atomically dispersed Au, as seen in Figure 4d, e, and f and Supporting Information Figure S2, confirming that the CH_3I treatment does result in significant dispersion of the Au material on the TiO_2 support. It should be noted that because of the very low visibility of these highly dispersed Au species against the much thicker TiO_2 crystallites and the strong dependence of their visibility on the precise crossover height of the convergent beam relative to the sample surface, it was not possible to quantify the number of these subnanometer clusters or isolated Au atoms in any statistically meaningful manner.

Figure 5 shows the *Z*-contrast HAADF images of the 0.9 wt % Au/Al_2O_3 catalyst in the "as-received" state and after CH_3I treatment. The "as-received" sample (Figure 5a and b, and Supporting Information Figure S3) consisted exclusively of 0.5−2.0 nm clusters (mean size 1.2 nm) homogeneously spread over the support. No atomically dispersed species were observed in the untreated sample. The CH_3I-treated sample (see Figure 6c−f and Supporting Information Figure S4) showed the presence of abundant atomically dispersed species as well as clusters in the 0.5−1.5 nm size range (mean size 1.0

dx.doi.org/10.1021/cs300074g | *ACS Catal.* 2012, 2, 552−560

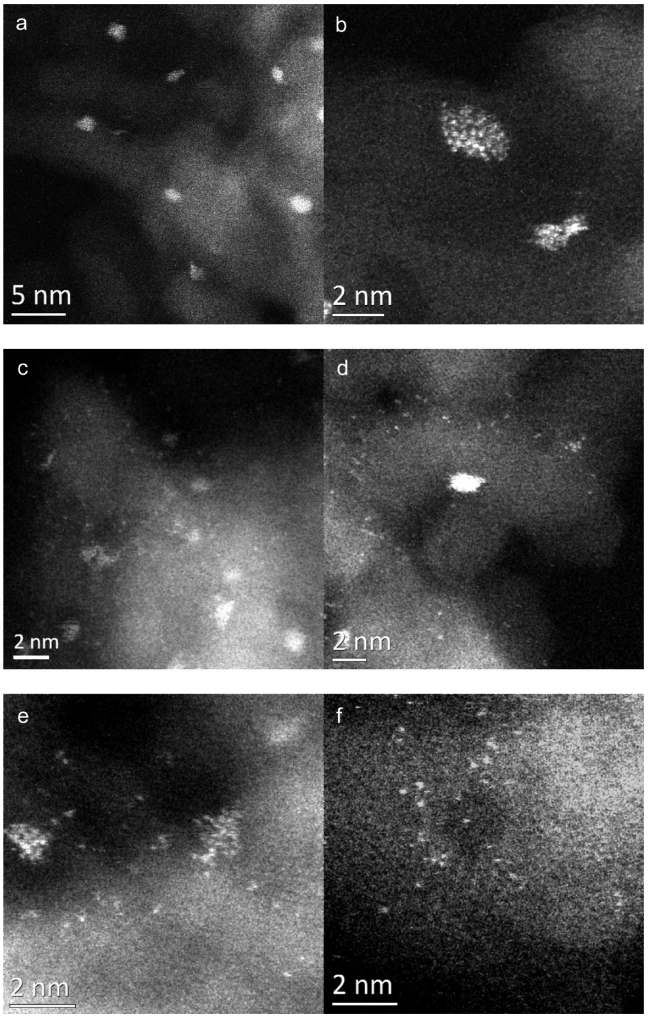

Figure 5. (a, b) Representative HAADF STEM images of the fresh 0.9 wt % Au/Al_2O_3 catalyst exclusively showing 0.5−2.0 nm clusters. (c−f) Corresponding images of the CH_3I-treated 0.9 wt % Au/Al_2O_3 material. It is clear that the 0.5−2.0 nm gold clusters have not been completely eradicated, but some have become disrupted and redistributed as atomically dispersed gold species.

nm), which is in good agreement to the DR-UV−vis results described below. This confirms that the CH_3I treatment had been partially successful in the dispersion of the Au on Al_2O_3 surface.

Figure 6 shows representative *Z*-contrast HAADF images of the 1.3 wt % Au/SiO_2 catalyst in the "as-received" state and after CH_3I treatment. Unlike the samples on TiO_2 or Al_2O_3 supports, there were very few nanometer-scale Au particles and no atomically dispersed species present on either the untreated or CH_3I-treated SiO_2 supports. This is consistent with other reports in which it has proven difficult to obtain a good dispersion of Au on SiO_2 by impregnation methods.[22] To locate the whereabouts of the Au in the SiO_2-based catalysts, they were also examined at much lower magnification using backscattered electron imaging in an SEM. As shown in Figure 7, it becomes apparent for both samples that the vast majority of the Au exists as much larger particles, in the 0.05−0.5 μm size range. Interestingly, the mean particle size was 0.20 μm for the untreated sample, which decreased to 0.16 μm after the CH_3I treatment. The respective particle size distributions are also presented in Figure 7 and clearly illustrate that a significant

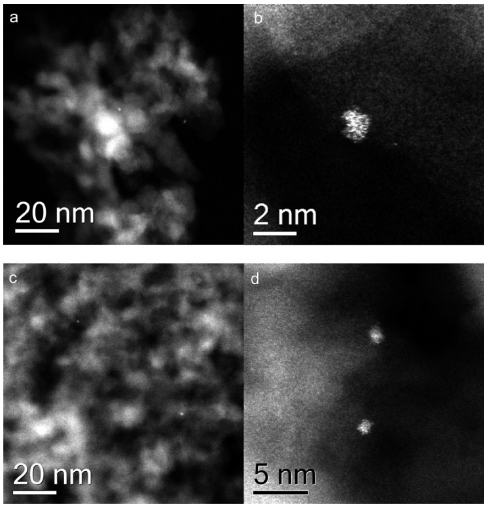

Figure 6. Representative HAADF STEM images (a, b) of the fresh 1.3 wt % Au/SiO_2 catalyst and (c, d) the corresponding CH_3I-treated material. In both cases, Au nanoparticles were very rarely found on the SiO_2 support.

degree of Au redispersion, albeit not on the nanometer scale, had still occurred on silica as a result of the CH_3I treatment.

XRD patterns of the 1.7 wt % Au/TiO_2, 2.0 wt % Au/Al_2O_3, and 1.3 wt % Au/SiO_2 catalysts are presented in Figures 8, 9, and 10, respectively. In all three cases, an intensity decrease and corresponding broadening of the Au(111) and (200) diffraction features occurs following the CH_3I treatment, which is consistent with significant dispersion of the gold nanoparticles into smaller species. Furthermore, the extent of metal dispersion follows the trend alumina > titania > silica catalysts, which is consistent with the DR-UV−vis and electron microscopy results.

Correlating the DR-UV−vis, XRD, and XPS results implies that the extent of gold dispersion achieved following the CH_3I treatment on the different supports may be related to the amount of residual surface iodine detected by XPS on the post-treatment samples (Table 1). As the surface concentration of iodine observed increases, the extent of dispersion found for the gold species also increases. Such behavior could be associated with a possible role of the support in activating the methyl iodide before the iodine reacts with the gold particles. Increasing the dispersion of the gold should result in an increase in the XPS Au 4f features; however, this occurs only for the 2.0 wt % Au/Al_2O_3 catalyst. The fact that the XPS shows a decrease in the Au 4f features following CH_3I treatment in most of the catalysts studied may be due to the surface coverage of iodine, diffusion of gold into the pores of the support, or both. The measured change in the size distribution of the gold particles, while remaining on the micrometer scale would also explain the fact that the silica catalyst shows little change in the Au 4f peak intensity.

To assess whether the catalysts had retained catalytic activity following the CH_3I treatment due to the presence of surface iodine, two test reactions were carried out: namely, benzyl alcohol oxidation and ethanol dehydrogenation. Both reactions have been shown to have a significant dependence on the catalyst activity on the gold particle size and, hence, were used to study the activity changes following dispersion of the gold. It should be noted that although the changes observed may be understood by changes in the gold particle size, it cannot be

dx.doi.org/10.1021/cs300074g | *ACS Catal.* 2012, 2, 552−560

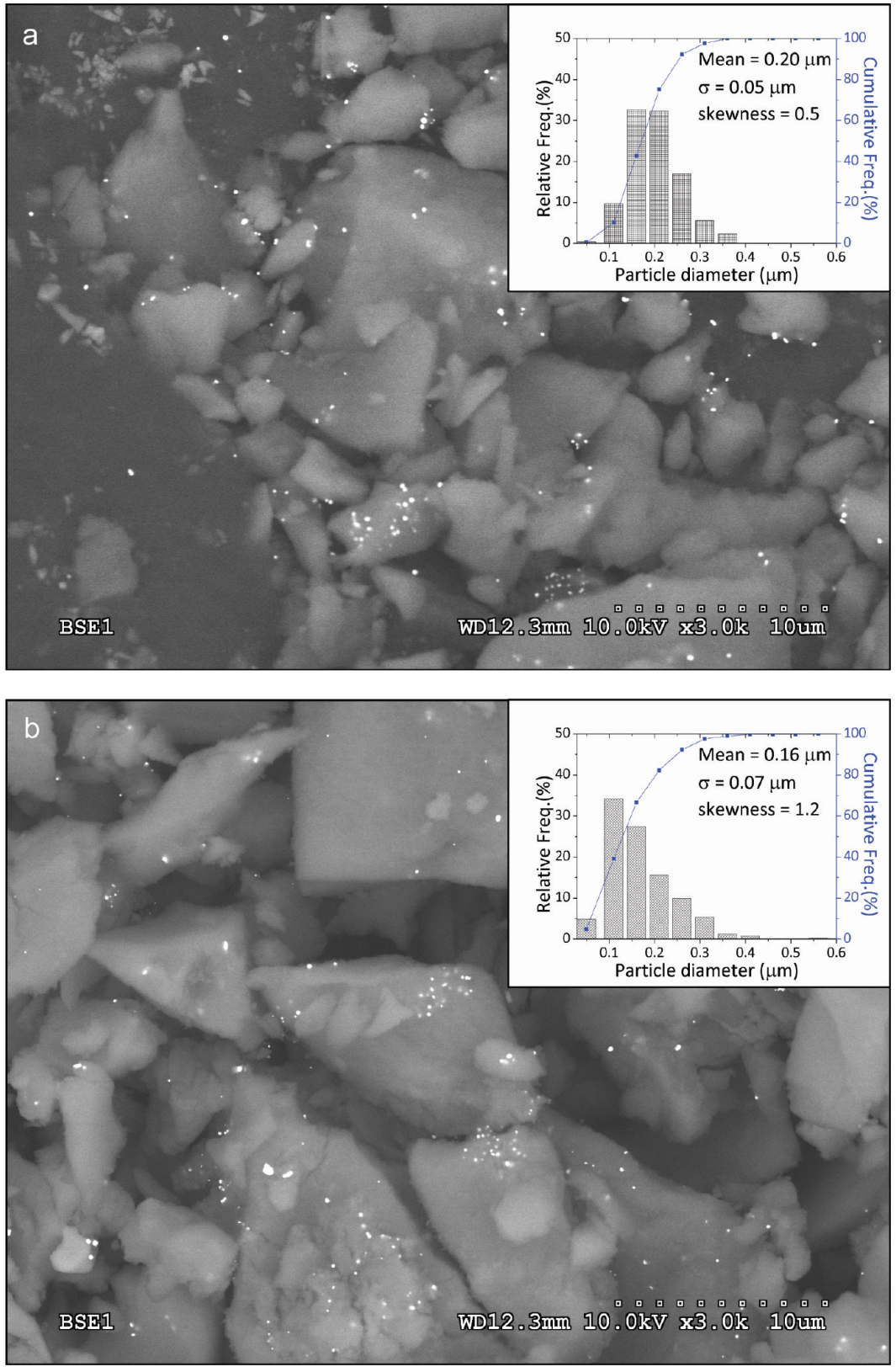

Figure 7. Representative SEM BSE images and corresponding particle size distributions (PSD) of (a) the fresh 1.3 wt % Au/SiO_2 catalyst and (b) the CH_3I-treated 1.3 wt % Au/SiO_2 material. The particle size histograms were derived from measurements of ~300 particles.

ruled out that the iodine present following the treatment could also contribute to the activity differences.

The catalytic performance of the fresh and CH_3I-treated catalysts for the aerobic oxidation of benzyl alcohol are reported in Table 2. For the fresh 0.8 wt % Au/TiO_2 catalyst, a conversion of 19.9% was found after 4 h reaction. This catalyst had a particle size similar to that reported to be optimum (~7 nm) for this reaction by Haider et al.,[23] but the

dx.doi.org/10.1021/cs300074g | ACS Catal. 2012, 2, 552−560

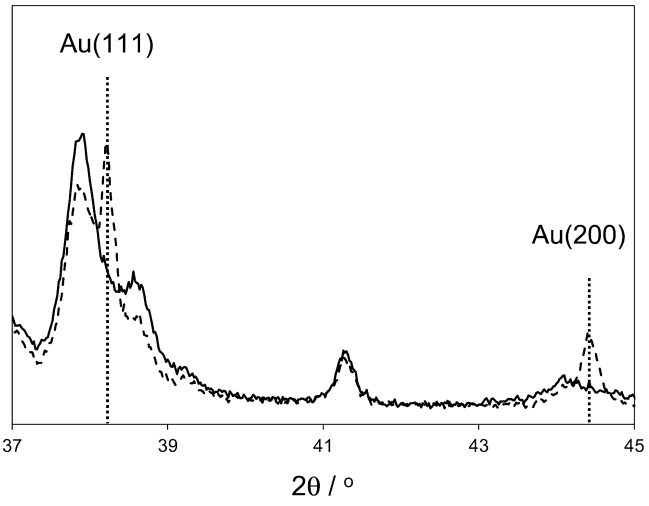

Figure 8. XRD of the 1.7 wt % Au/TiO_2 catalyst before (dashed line) and after (solid line) CH_3I treatment.

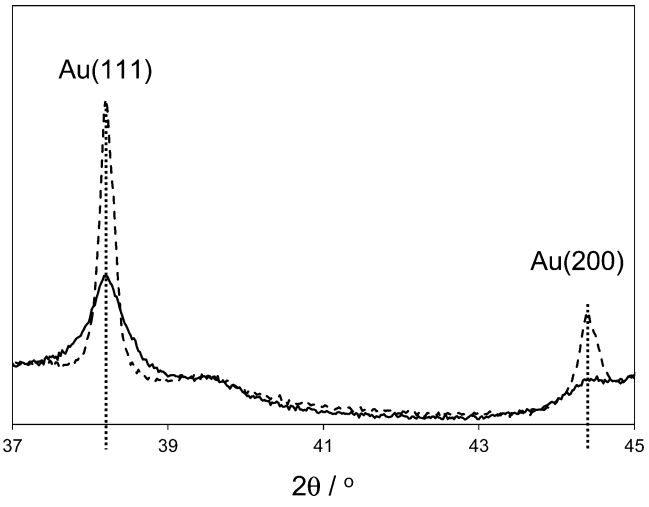

Figure 9. XRD of the 2.0 wt % Au/Al_2O_3 catalyst before (dashed line) and after (solid line) CH_3I treatment.

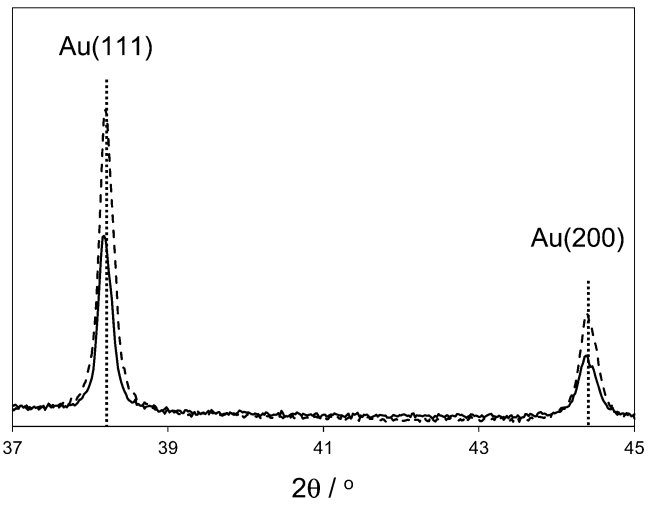

Figure 10. XRD of the 1.3 wt % Au/SiO_2 catalyst before (dashed line) and after (solid line) CH_3I treatment.

Table 2. Comparison of the Catalytic Activity and Selectivity in Benzyl Alcohol Oxidation at 80 °C after 4 h of the Pure Supports as well as the Fresh and CH_3I-Treated Supported Gold Catalysts

catalyst	conversion (%)	benzaldehyde yield (%)
TiO_2 P25	3.3	55.7
0.8Ti-fresh	19.9	88.4
0.8Ti-CH_3I	3.4	75.6
1.7Ti-fresh	0.3	1.1
1.7Ti-CH_3I	1.5	23.0
γ-Al_2O_3	5.8	0.0
0.9Al-fresh	93.4	89.5
0.9Al-CH_3I	5.4	18.1
2.0Al-fresh	2.9	20.7
2.0Al-CH_3I	2.3	32.8
SiO_2	2.4	48.9
1.3Si-fresh	2.3	28.8
1.3Si-CH_3I	2.4	4.8

conversion was approximately twice that reported previously, which is probably related to the higher loading of the catalyst used in the present study. In addition, the yield of benzaldehyde was ~88%, which is slightly lower than that previously reported.[23]

Upon CH_3I treatment, the conversion and benzaldehyde yield decreased to 3.4% and 76%, respectively. These results are consistent with those reported by Haider et al. who showed that smaller gold particles led to a decreased performance. In the case of the 0.9 wt % Au/Al_2O_3 catalysts, the measured trend was the same as that observed for the 0.8 wt % Au/TiO_2 catalysts. Following CH_3I treatment, a substantial decrease in both the conversion and selectivity was observed; however, in this case, the decrease was even higher than the case of the titania-supported material.

For all the catalysts with higher metal loadings, that is, 1.3 wt % Au/SiO_2, 1.7 wt % Au/TiO_2 and 2.0 wt % Au/Al_2O_3, the changes observed following CH_3I treatment are much smaller. For example, the activity of the fresh 1.7 wt % Au/TiO_2 catalyst was low in terms of both conversion (0.3%) and benzaldehyde yield (1.1%), which is consistent with the presence of large gold particles. Upon CH_3I treatment, the conversion increased to 1.5%, and the benzaldehyde yield, to 23%. Although the performance of the CH_3I-treated catalyst is still poor in this case, the results obtained clearly show that the gold redispersion treatment can lead to improved catalytic performance due to the decrease in the mean gold particle size.

The modest changes in performance and the overall poor catalytic activity/selectivity of all these catalyst following CH_3I treatment may be associated by the fact that small clusters and isolated atoms are formed, which are known to have poor activity and selectivity for this reaction. In addition, for the catalysts with high metal loadings, before the dispersion treatment, the gold particles are above optimal size, again leading to poor activity and selectivity. The data from the carbon-based catalysts previously reported indicated that the mechanism by which the CH_3I led to dispersion of the gold was that the CH_3I gradually reacts with the surface gold atoms, gradually reducing the particle size and forming small gold iodide complexes.[16] Given this mechanism and assuming that a similar process takes place on the oxide-supported catalysts, it is unlikely that simply using the CH_3I treatment will provide an efficient method by which to optimize the particle size.

dx.doi.org/10.1021/cs300074g | ACS Catal. 2012, 2, 552−560

Therefore, a two-stage process using the CH_3I to highly disperse the gold, followed by a subsequent thermal treatment to sinter the gold in a controlled manner, could be performed.

Ethanol dehydration catalyzed by gold is also known to be sensitive to the gold particle size. Guan and Hensen[24] observed an optimum turnover frequency (TOF) for this reaction over gold catalysts with an average particle size of 5 nm, whereas relatively low TOFs were found over gold catalysts with metal particle sizes of 1.7 nm. The catalytic performance for ethanol dehydration of the catalysts studied (Table 3) shows that all the

Table 3. Catalytic Performance Shown for Ethanol Dehydration at 400 °C after 1 h

catalyst	conversion (%)	yield of methanal (%)	yield of ethene (%)	ratio of methanal/ethene
TiO_2 P25	34.3	4.3	18.7	0.23
0.8Ti-fresh	39.6	4.1	20.0	0.21
0.8Ti-CH_3I	50.4	2.9	17.8	0.16
1.7Ti-fresh	33.6	3.3	14.3	0.23
1.7Ti-CH_3I	38.0	3.8	14.8	0.26
γ-Al_2O_3[a]	78.4	0.0	36.1	0.00
0.9Al-fresh[a]	46.9	0.0	15.4	0.00
0.9Al-CH_3I[a]	19.6	1.8	16.5	0.11
2.0Al-fresh	27.3	0.0	17.4	0.00
2.0Al-CH_3I	33.4	0.0	18.8	0.00
SiO_2	3.7	0.9	2.8	0.32
1.3Si-fresh	4.9	1.2	3.6	0.33
1.3Si-CH_3I	4.4	1.1	3.3	0.33

[a]300 °C was used as the reaction temperature because of the very high conversions found at 400 °C.

catalysts exhibit high selectivity to the dehydration products (ethene and water), with small amounts of methanal and hydrogen due to reforming processes. This selectivity is in contrast to those results reported by Guan and Hensen, in which ethanal was found to be the main product. In general, increased conversion was found following the CH_3I treatment, with the two exceptions to this being (i) the 0.9 wt % Au/Al_2O_3 catalyst, in which a decrease in conversion is found, and (ii) the silica-supported catalyst, whose catalytic activity is initially poor and did not change significantly on CH_3I treatment. The results obtained with the 0.9 wt % Au/Al_2O_3 catalyst are consistent with the fact that this catalyst has the smallest metal particles in the fresh catalyst, with a previously reported average particle size between 1 and 3 nm from the electron microscopy, which is similar to the optimal size of 5 nm reported previously.[24] Following dispersion of the gold, the surface consists of a considerable amount of atomically dispersed and subnanometer clusters, both of which correspond to poorly active gold morphologies. In the case of the silica-based catalyst, the result is consistent with the large gold particles for the fresh catalyst and limited dispersion response to the methyl iodide treatment, leading to no catalytic improvement after the treatment.

CONCLUSIONS

The reported results show the applicability of CH_3I treatments for the dispersion of gold particles on oxide supports. The extent of the redispersion is strongly influenced by the identity of the oxide support, with alumina-based catalysts showing the largest change in the gold metal particle size and silica-based systems showing only a weak response to the CH_3I treatment. In most cases, the CH_3I treatment resulted in a significant change in the catalytic performance in both benzyl alcohol oxidation and ethanol dehydration reactions with, in all cases, the catalyst shown to have activity following the CH_3I treatment. Although not producing an optimized catalyst, some improvements in the activity and selectivity performance of the catalysts were observed compared with the fresh catalyst. It is likely that optimization of the catalytic performance would be achieved by using a mild CH_3I treatment for dispersion of the gold *followed* by controlled thermal/hydrothermal sintering of the gold. In addition, the methyl iodide treatment provides a method of reactivating gold catalysts that have been deactivated by sintering or loss of the metal−support interaction.

ASSOCIATED CONTENT

Supporting Information

Additional STEM-HAADF images and a particle size distribution histogram for the untreated and CH_3I treated Au/TiO_2 and Au/Al_2O_3 catalysts. This material is available free of charge via the Internet at http://pubs.acs.org.

AUTHOR INFORMATION

Corresponding Author

*E-mail: c.hardacre@qub.ac.uk.

Notes

The authors declare no competing financial interest.

ACKNOWLEDGMENTS

We acknowledge EPSRC for funding under the CASTech grant.

REFERENCES

(1) Bond, G.; Louis, C.; Thompson, D. T. *Catalysis by Gold*; Imperial College Press; Catal. Sci. Series 2006, Vol. 6.
(2) Haruta, M.; Kobayachi, T.; Sano, H.; Yamada, N. *Chem. Lett.* **1987**, *2*, 405−408.
(3) Hutchings, G. J. *J. Catal.* **1985**, *96*, 292−295.
(4) Corma, A.; González-Arellano, C.; Iglesias, M.; Sánchez, F. *Appl. Catal., A* **2009**, *356*, 99−102.
(5) Biella, S.; Prati, L.; Rossi, M. *J. Catal.* **2002**, *206*, 242−247.
(6) Corma, A.; Concepción, P.; Domínguez, I.; Fornés, V.; Sabater, M. J. *J. Catal.* **2007**, *251*, 39−47.
(7) Corma, A.; Domínguez, I.; Doménech, A.; Fornés, V.; Gómez-García, C. J.; Ródenas, T.; Sabater, M. J. *J. Catal.* **2009**, *265*, 238−244.
(8) Magureanu, M.; Mandache, N. B.; Hu, J.; Richards, R.; Florea, M.; Parvulescu, V. I. *Appl. Catal., B* **2007**, *76*, 275−281.
(9) Corti, C. W.; Holliday, R. J.; Thompson, D. T. *Appl. Catal., A* **2005**, *291*, 253−261.
(10) Abad, A.; Concepcion, P.; Corma, A.; Garcia, H. *Angew. Chem., Int. Ed.* **2005**, *44*, 4066−4069.
(11) Biella, S.; Rossi, M. *Chem. Commun.* **2003**, 378−379.
(12) Guzman, J.; Gates, B. C. *J. Am. Chem. Soc.* **2004**, *126*, 2672−2673.
(13) Goguet, A.; Burch, R.; Chen, Y.; Hardacre, C.; Hu, P.; Joyner, R. W.; Meunier, F. C.; Mun, B. S.; Thompsett, D.; Tibiletti, D. *J. Phys. Chem. C* **2007**, *111*, 16927−16933.

(14) Zoeller, J. R.; Singleton, A. H.; Tustin, G. C.; Carver, D. L. U.S. Patents Nos. 6,506,933 and 6,509,293.
(15) Goguet, A.; Hardacre, C.; Harvey, I.; Narasimharao, K.; Saih, Y.; Sá, Y. *J. Am. Chem. Soc.* **2009**, *131*, 6973−6975.
(16) Sá, J.; Taylor, S. F. R.; Paun, C.; Goguet, A.; Tiruvalam, R.; Kiely, C. J.; Nachtegaal, M.; Hutchings, G.; Hardacre, C. *Angew. Chem., Int. Ed.* **2011**, *50*, 8912−8916.
(17) http://www.gold.org.
(18) Kitagawa, H.; Kojima, N.; Nakajima, T. *J. Chem. Soc., Dalton Trans.* **1991**, 3121−2125.
(19) Smolentseva, E.; Bogdanchikova, N.; Simakov, A.; Pestryakov, A.; Tusovskaya, I.; Avalos, M.; Farías, M. H.; Díaz, J. A.; Gurin, V. V. *Surf. Sci.* **2006**, *600*, 4256−4259.
(20) Tuzovskaya, I. V.; Simakov, A. V.; Pestryakov, A. N.; Bogdanchikova, N. E.; Gurin, V. V.; Farías, M. H.; Tiznado, H. J.; Avalos, M. *Catal. Commun.* **2007**, *8*, 977−9780.
(21) Raphulu, M.; McPherson, J.; Pattrick, G.; Ntho, T.; Mokoena, L.; Moma, J.; van der Lingen, E. *Gold Bull.* **2009**, *42*, 328−336.
(22) Okumura, M.; Nakamura, S.; Tsubota, S.; Nakamura, T.; Haruta, M. *Stud. Surf. Sci. Catal.* **1998**, *118*, 277−284.
(23) Haider, P.; Kimmerle, B.; Krumeich, F.; Kleist, W.; Grunwaldt, J.-D.; Baiker, A. *Catal. Lett.* **2008**, *125*, 169−176.
(24) Guan, Y.; Hensen, E. J. M. *Appl. Catal., A* **2009**, *361*, 49−56.